

Mapping the molecular surface of the analgesic Nav1.7-selective peptide Pn3a reveals residues essential for membrane and channel interactions

Alexander Mueller^a, Zoltan Dekan^a, Quentin Kaas^a, Akello J. Agwa^{a,§}, Hana Starobova^a, Paul F. Alewood^a, Christina I. Schroeder^a, Mehdi Mobli^b, Jennifer R. Deuis^{a,*,1} and Irina Vetter^{a,c,*,2}

^aInstitute for Molecular Bioscience, The University of Queensland, St. Lucia, QLD 4072, Australia

^bCentre for Advanced Imaging, The University of Queensland, St. Lucia, QLD 4072, Australia

^cSchool of Pharmacy, The University of Queensland, Woolloongabba, QLD 4102, Australia

* Co-corresponding authors

¹Address: Institute for Molecular Bioscience, The University of Queensland, 306 Carmody Rd, St Lucia, Queensland 4072, Australia. Tel.: +617 3346 2721; E-mail: j.deuis@uq.edu.au

²Address: Institute for Molecular Bioscience, The University of Queensland, 306 Carmody Rd, St Lucia, Queensland 4072, Australia. Tel.: +617 3346 2660; fax: +61 733 462 101; E-mail: i.vetter@uq.edu.au

[§] Current address: University of Bath, Department of Biology and Biochemistry, BA27AY, Bath, UK.

Keywords:

Structure-activity relationship, Peptide synthesis, Voltage-gated sodium channel 1.7, Gating-modifier toxin, Pharmacophore, Pain.

Abstract

Compelling human genetic studies have identified the voltage-gated sodium channel Nav_v1.7 as a promising therapeutic target for the treatment of pain. The analgesic spider venom-derived peptide μ -theraphotoxin-Pn3a is an exceptionally potent and selective inhibitor of Nav_v1.7, however, little is known about the structure-activity relationships or channel interactions that define this activity. We rationally designed seventeen Pn3a analogues and determined their activity at hNav_v1.7 using patch-clamp electrophysiology. The positively charged amino acids K22 and K24 were identified as crucial for Pn3a activity, with molecular modeling identifying interactions of these residues with the S3-S4 loop of domain II of hNav_v1.7. Removal of hydrophobic residues Y4, Y27 and W30 led to a loss of potency (>250-fold), while replacement of negatively charged D1 and D8 residues with a positively charged lysine led to increased potencies (>13-fold), likely through alterations in membrane lipid interactions. Mutating D8 to an asparagine led to the greatest improvement in Pn3a potency at Nav_v1.7 (20-fold), whilst maintaining >100-fold selectivity over the major off-targets Nav_v1.4, Nav_v1.5 and Nav_v1.6. The Pn3a[D8N] mutant retained analgesic activity *in vivo*, significantly attenuating mechanical allodynia in a clinically relevant mouse model of post-surgical pain at doses 3-fold lower than wild-type Pn3a, without causing motor adverse effects. Results from this study will facilitate future rational design of potent and selective peptidic Nav_v1.7 inhibitors for the development of more efficacious and safer analgesics but also to further investigate the involvement of Nav_v1.7 in pain.

Pain remains a poorly treated condition with currently used analgesics often suffering from poor tolerability, abuse potential or lack of broad efficacy ¹. The voltage-gated sodium channel isoform Nav1.7 is considered one of the most promising validated pain targets, with loss-of-function mutations leading to Congenital Insensitivity to Pain (CIP) ², while gain-of-function mutations are associated with a range of painful conditions ³⁻⁵. As CIP is characterized by a lack of nociception, with no other significant autonomic or sensory impairments apart from anosmia ⁶, targeting Nav1.7 pharmacologically promises to deliver effective analgesia without substantial side effects. Accordingly, intense research efforts have been devoted to the identification of subtype-selective Nav1.7 modulators ^{7,8}. Nevertheless, this endeavor has proven challenging, not least owing to the high degree of similarity of the Nav subtypes, especially in the pore domain where many clinically used Nav modulators bind ⁶.

One particularly promising source of selective Nav modulators are animal venoms, which are typically dominated by small (~20–40 amino acids) peptides that target the voltage-sensing domains (VSDs) of Nav channels ⁹⁻¹¹. Specifically, several spider venom-derived peptides target the VSDII to stabilize the “down” or resting/closed state of the channel, leading to a depolarizing shift in the voltage-dependence of channel activation ^{12,13}. Analogous to small molecules binding to VSDIV of Nav1.7 ¹⁴, targeting the voltage-sensors of domain II imparts a typically greater degree of selectivity compared to targeting the pore domain, with many spider venom-derived peptides displaying excellent selectivity over tetrodotoxin (TTX)-resistant isoforms including the cardiac isoform Nav1.5, a major pharmacological off-target ⁶. However, selectivity for Nav1.7 over the TTX-sensitive isoforms is often more limited, with few potent and truly selective molecules reported ¹⁵⁻¹⁷. These include the prototypical Nav1.7-targeting peptide toxin Protoxin-II (ProTx-II or β/ω -theraphotoxin-Tp2a) from the venom of the tarantula *Thrixopelma pruriens*

¹⁸, rationally engineered analogues of Jingzhaotoxin-V (JzTx-V, β/κ -theraphotoxin-Cg2a) ¹⁹ and GpTx-1 (ω -theraphotoxin-Gr2a) ²⁰, as well as the recently described analgesic peptide Pn3a (μ -theraphotoxin-Pn3a) from the venom of the tarantula *Pamphobeteus nigricolor* ^{21, 22}. Notably, these Nav1.7 inhibitors belong to diverse peptide families of Nav channel targeting spider-venom toxins (NaSpTx families 1-3), based on sequence similarities ^{17, 23}. Extensive structure-activity studies have been described for NaSpTx family 3 peptides, which include JzTx-V and ProTx-II ^{17, 19, 24, 25}, as well as for NaSpTx family 1 peptides, which include GpTx-1 ^{17, 20, 26}. However, so far nothing is known about the structural features that confer activity at Nav1.7 for the NaSpTx family 2 peptides, to which Pn3a belongs. Pn3a is one of the most potent and selective reported Nav1.7 blockers and inhibits Nav1.7 with several hundred-fold selectivity over the key TTX-sensitive off-targets Nav1.4 and Nav1.6, and is analgesic either alone or in combination with oxycodone or baclofen in multiple animal models of pain ^{21, 22}.

Thus, the goal of this study was to investigate the structure-activity relationships of Pn3a using rational analogue design to better understand the features necessary for potent inhibition of Nav1.7. We confirmed the importance of a key phenylalanine residue near the S3-S4 loop of Nav1.7 VSDII (F823) for peptide activity and identified several Pn3a amino acid residues crucial for potency, selectivity and membrane binding. Improved *in vivo* antinociceptive efficacy of Pn3a[D8N] was confirmed in a Nav1.7 target engagement assay as well as a mouse model of post-surgical pain. These results will guide future rational design of potent and selective Nav1.7 inhibitors as more efficacious and safer analgesics.

1. Results and Discussion

1.1 F823 in VSDII of Nav1.7 is a key residue for interaction with Pn3a

Pn3a is the only Nav1.7-selective inhibitor belonging to NaSpTx family 2 reported to date, with most other members of this family inhibiting voltage-gated potassium (K_v) channels, or acting as functional Na_v activators. Specifically, the most closely related NaSpTx family 2 Na_v modulator SGTx1 (κ -theraphotoxin-Scg1a), sharing 22 identical residues and a very similar 3D backbone structure with Pn3a, is a non-selective Na_v activator and K_v2.1 inhibitor^{27, 28} (**Fig 1A**). Similarly, the closely related family 2 peptides Hm1a and Hm1b (δ -theraphotoxin-Hm1a and δ -theraphotoxin-Hm1b) selectively inhibit inactivation of Nav1.1 but have no effect on Nav1.7²⁹ (**Fig. 1A**). In contrast, the pharmacologically most similar spider venom-derived peptide to Pn3a is ProTx-II, a selective NaSpTx family 3 Nav1.7 blocker with a well described pharmacophore^{12, 30, 31}. However, ProTx-II has little sequence similarity to Pn3a (**Fig. 1A**), and although we have previously demonstrated that Nav1.7 inhibition by Pn3a involves binding to the S3-S4 loop of VSDII, we first sought to verify that Pn3a and ProTx-II share an overlapping binding site. ProTx-II has previously been shown to bind to F823 (mNav1.7; F813 hNav1.7) in the S3-S4 loop of VSDII (ELFLADVEG), with a F823→G mutation reducing ProTx-II inhibitory activity by between 9–100-fold^{18, 32}. This interaction was also confirmed by recent structural studies¹² which additionally suggest that besides Van der Waals interactions of F823 with hydrophobic ProTx-II residues, this Nav1.7-specific residue may be important for S3 helix stabilization as well as for S3-S4 loop orientation in VSDII to provide a Nav1.7-specific receptor site.

We therefore assessed the potency of Pn3a at a F823G mutant of Nav1.7 and found that, as expected, Pn3a was 28-fold less active at mutant (IC₅₀ 293.4 nM) compared to wild-type channels (IC₅₀ 10.4 nM) (**Fig. 1B**), suggesting an overlapping binding site of Pn3a and ProTx-II at VSDII.

1.2 Comparison of the primary and tertiary structure of Pn3a to spider venom-derived Nav modulators

To identify amino acids that might confer Nav1.7 selective inhibition, we used a systematic approach based on aligning and comparing the primary (**Fig. 1A**) and tertiary structures of Pn3a with structurally closely related spider venom peptides (SGTx1, Hm1a and Hm1b) (**Fig. 1C**) as well as the pharmacologically similar ProTx-II (**Fig. 1D**), despite obvious differences in the sequences. Our sequence and structural alignments revealed several interesting commonalities and differences, including several charge substitutions in Pn3a compared to Hm1b and ProTx-II (D8, D12, E10, E13 and K24); as well as a structurally conserved arrangement of key hydrophobic residues (Y4, Y27, W30) (**Fig. 1A and D**). Thus, overall, Pn3a has a conserved amphipathic surface structure with a hydrophobic patch surrounded by charged residues (**Fig. 1E**), which is thought to permit membrane partitioning as well as interaction with parts of the VSDs located close to the extracellular surface^{12, 33, 34}. Therefore, to delineate the contributions of these residues to Pn3a activity, we next pharmacologically characterized select peptide analogues.

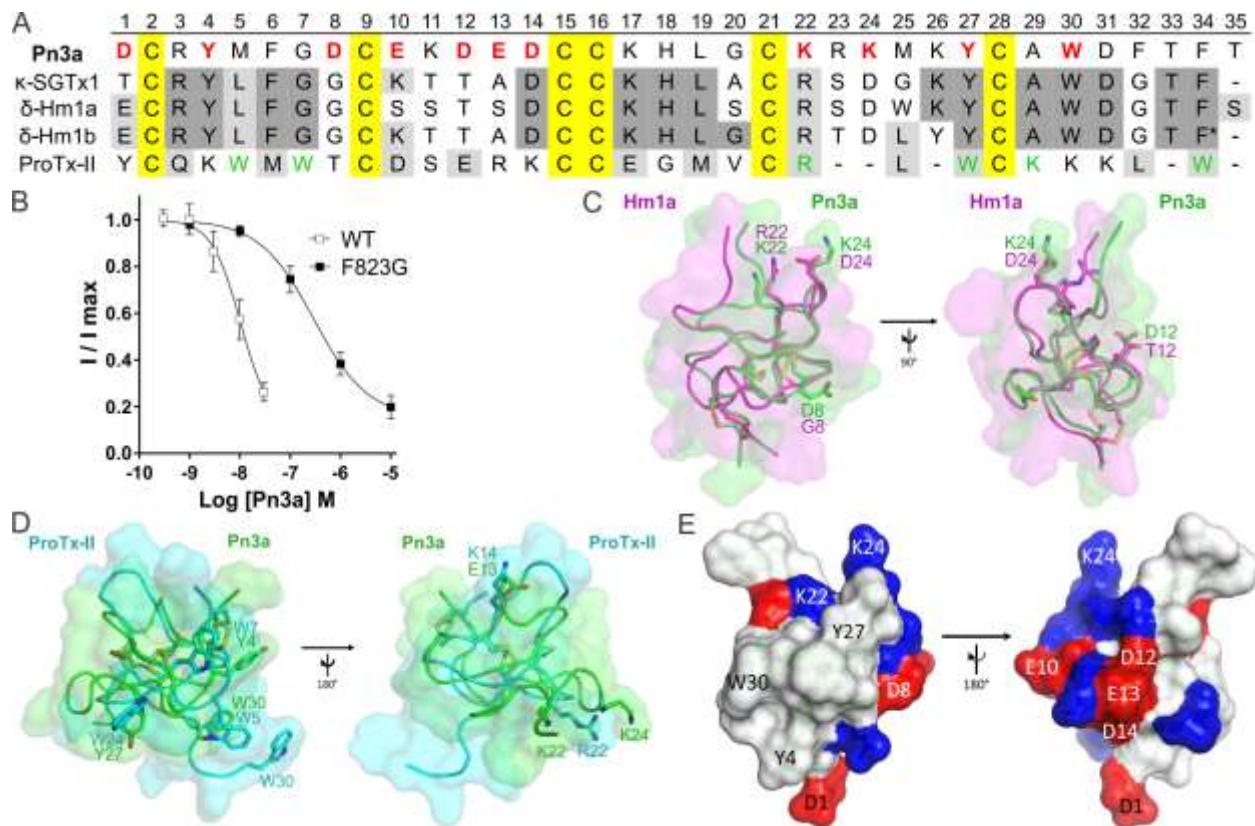


Figure 1. Sequence and structural features of Pn3a (A) Amino acid sequence alignment of Pn3a with closely related venom peptides κ -SGTx1, δ -Hm1a, δ -Hm1b and ProTx-II. Yellow shading indicates cysteines; dark grey and light grey shading represents identical and similar amino acids, respectively compared to Pn3a; red bold letters indicate residues included in SAR study; green letters indicate pharmacophore residues in ProTx-II for $\text{Na}_v1.7$ activity^{12, 30, 31}. * indicates amidated C-terminus of Hm1b. (B) Pn3a is 28-fold more potent at wild-type $\text{mNa}_v1.7$ (IC_{50} 10.4 nM) compared to $\text{mNa}_v1.7$ [F823G] (IC_{50} 293.4 nM) mutant channels assessed by whole-cell patch-clamp experiments. Data are presented as mean \pm SEM, with $n = 5-9$ cells per data point. (C) Comparison of NMR structures of Pn3a (PDB 5T4R; green) with Hm1a (PDB 2N6O; pink) superimposed over the disulfide bonds (yellow), generated with PyMol. Residues of interest are labelled and shown in stick-representation. (D) Comparison of NMR structures of Pn3a (PDB 5T4R; green) with ProTx-II (PDB 2N9T; cyan) superimposed over the disulfide bonds (yellow). Overlapping residues with similar chemical properties are labelled and shown as sticks. (E) Surface structure of Pn3a with acidic and basic residues highlighted in red and blue, respectively. The hydrophobic patch (including W30, Y4 and Y27) is surrounded by a charged ring (including D1, D8, K22 and K24; left), while the reverse side is hydrophilic with mainly charged side chains (right). Only residues included in this SAR study are labelled.

1.3 The conserved hydrophobic patch of Pn3a contributes to activity and peptide folding

Based on the observed overlap of Y4, Y27 and W30 in Pn3a with W7, W24 and W5, respectively, in ProTx-II (**Fig. 1D**), we first characterized the contribution of these hydrophobic patch residues to Pn3a activity. Mutations of all three residues to alanine resulted in at least 250-fold reduced potency at Nav1.7 (IC₅₀ values > 1 μM) compared to Pn3a (IC₅₀ 4 nM) (**Fig. 2A, Table 1**), although the isolated predominant isomer obtained for Pn3a[Y27A] was in a non-native fold as determined by 1D NMR (**Fig. S1**). A similar contribution of this residue to folding of SGTx1 has previously been reported, with the SGTx1[Y27A] mutant lowering folding efficiency and preventing identification of correctly folded peptide³⁵. Interestingly, hydrophobic patch residues are also critical for potency of ProTx-II and appear to anchor the peptide in the membrane-embedded lipophilic cleft at the S2 and S3 interface just above F813 of VSDII in hNav1.7^{12,31}. These results suggest that Pn3a may employ a similar binding mode to ProTx-II with hydrophobic patch residues directly interacting with Nav1.7, and confirm Y4 and W30 as part of the pharmacophore and Y27 as important structural feature for native folding of Pn3a.

1.4 K22 and a basic residue at position 24 are essential for inhibition of Nav1.7

R22 in ProTx-II is critical for its potency and has been shown to directly interact with acidic residues in the extracellular S3-S4 loop of Nav1.7 VSDII, antagonizing S4 gating-charge movement to prevent channel opening¹². Interestingly, K22 and K24 in Pn3a flank the corresponding position of R22 in ProTx-II and are located in close proximity, although neither directly overlap with this crucial pharmacophore residue (**Fig. 1D**). We therefore assessed activity of charge-neutral K22 and K24 analogues (K22A and K24A) as well as the corresponding arginine

mutants (K22R and K24R) and the negatively charged analogue (K24D) which additionally mirrors the sequence of the family 2 Nav activators SGTx1, Hm1a and Hm1b in this position (**Fig. 1A and C**).

As expected, both K24A (IC_{50} 84 nM) and K22A ($IC_{50} > 1 \mu\text{M}$) lost activity at Nav1.7, although substitution of K24 appears better tolerated than replacement of K22, with 21-fold and > 250 -fold loss of potency, respectively (**Fig. 2B, Table 1**). Similarly, substitution of K22 with arginine led to a 6-fold decrease in potency (IC_{50} 24 nM), while K24R (IC_{50} 1 nM) gained 4-fold potency compared to Pn3a, suggesting that the lysine at position 22 and a basic residue at position 24 in Pn3a are important for potent Nav1.7 channel inhibition (**Fig. 2B, Table 1**). The bulkier arginine at position 22 in Pn3a may be sterically unfavorable for channel engagement, while position 24 seems more tolerant to modifications and Nav1.7 may better accommodate an arginine at position 24 for more potent channel inhibition.

Interestingly, the Nav activators SGTx1, Hm1a and Hm1b all contain an aspartic acid at position 24 (**Fig. 1A**), suggesting this residue may be an important feature for the different pharmacological profiles. Indeed, consistent with a voltage-sensor trapping model involving electrostatic interactions between charged residues of toxins and the VSD, we hypothesized that the K24D substitution might impart Nav activator properties on Pn3a. However, while the Pn3a[K24D] analogue lost > 250 -fold potency at Nav1.7 ($IC_{50} > 1 \mu\text{M}$) (**Fig. 2B, Table 1**), we neither observed increases in peak currents, hyperpolarizing shifts in the voltage-dependence of activation, or delayed inactivation at either Nav1.1 and Nav1.7 channels (**Fig. S2**). Given that effects on inactivation are typically mediated via interaction with the VSD of domain IV, while effects on activation are commonly mediated via VSDII interactions, it is perhaps not surprising that this single residue substitution did not convert Pn3a into a Nav activator, but only prevented potent

inhibition of channel activation. Further VSDIV interactions that would interfere with channel inactivation (similar to SGTx1, Hm1a and Hm1b effects) may require additional mutations to Pn3a. Nevertheless, our findings indicate that the presence of D24 in Hm1a/b and SGTx1 may prevent these peptides from being Nav channel blockers by preventing close interaction with acidic VSDII S3-S4 loop residues. Indeed, the D24A mutation in SGTx1 has been shown to result in a ~20-fold reduction of the K_d value compared to wild-type peptide³⁵. Future studies are needed to investigate if a single amino acid exchange to a basic residue at position 24 can turn these Nav activators into blockers.

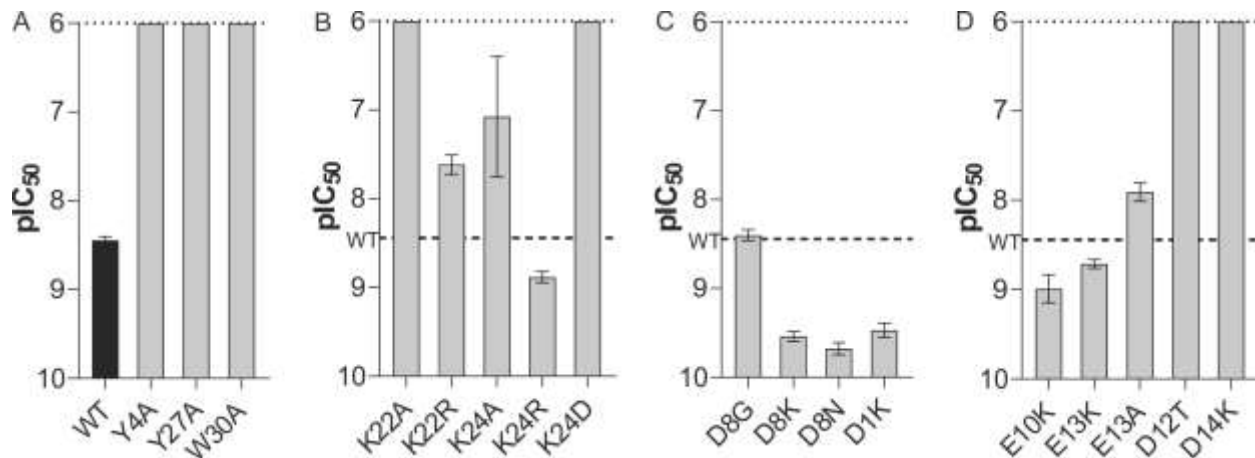


Figure 2. Activity of Pn3a mutants at hNav1.7 assessed by whole-cell patch-clamp experiments. **(A)** Potency of Pn3a (WT) and the surface hydrophobic patch analogues Y4A, Y27A and W30A. Note: Y27A is in a non-native fold. **(B)** Potency of analogues with mutations at position 22 and 24. **(C)** Potency of charged ring analogues D8G, D8K, D8N and D1K. **(D)** Potency of Pn3a analogues E10K, E13K, E13A, D12T and D14K. Note: D12T and D14K are in a non-native fold. Dotted line indicates maximal tested concentration of 1 μ M. Dashed line indicates potency of wild-type Pn3a. Data are presented as mean \pm SEM, with n = 3–9 cells per data point.

Table 1: Potency of Pn3a analogues at hNav1.7. pIC₅₀ (expressed as mean ± SEM) and IC₅₀ values of Pn3a (WT) and Pn3a-analogues derived from concentration-response relationships assessed by whole-cell patch-clamp experiments. * = non-native fold assessed by 1D NMR; all other analogues showed a similar fold to WT peptide.

Pn3a analogue	pIC₅₀ [M]	IC₅₀ [nM]
WT	8.45 ± 0.04	4
D1K	9.47 ± 0.08	0.3
Y4A	< 6	> 1000
D8K	9.54 ± 0.06	0.3
D8N	9.68 ± 0.07	0.2
D8G	8.40 ± 0.06	4
E10K	8.99 ± 0.16	1
D12T *	< 6	> 1000
E13K	8.71 ± 0.05	2
E13A	7.91 ± 0.10	12
D14K *	< 6	> 1000
K22A	< 6	> 1000
K22R	7.62 ± 0.11	24
K24A	7.08 ± 0.68	84
K24D	< 6	> 1000
K24R	8.88 ± 0.06	1
Y27A *	< 6	> 1000
W30A	< 6	> 1000

1.5 Removal of negative charges improves Pn3a potency

Pn3a contains a number of negatively charged residues differentiating it from both the NaSpTx family 2 Nav activators as well as ProTx-II, including D1, D8, E10, D12, E13 and D14 (**Fig. 1A**). To explore the contributions of these residues to Pn3a activity, we generated a range of analogues based on charge neutralizing or charge reversing substitutions. Pn3a[D8G] – analogous to the corresponding residue in SGTx1, Hm1a and Hm1b – remained equipotent (IC₅₀ 4 nM) in patch-clamp experiments. Surprisingly, D8N (IC₅₀ 0.2 nM) and D8K (IC₅₀ 0.3 nM) displayed a 20-fold and 13-fold improved potency at Nav1.7 compared to wild-type Pn3a, respectively (**Fig. 2C, Table 1**). This suggests that a positive or polar-neutral residue at position 8 in Pn3a allows for better inhibition of the channel, possibly due to facilitation of direct Nav channel interactions or through

advantageous membrane binding properties. Similarly, the potency of Pn3a[D1K] (IC_{50} 0.3 nM) was improved 13-fold (**Fig. 2C, Table 1**).

The position corresponding to Pn3a E10 is occupied by a lysine residue in Hm1b, while E13 in Pn3a overlays well with the oppositely-charged K14 in ProTx-II and an alanine residue in Hm1b (**Fig. 1A and D**). We therefore also generated E10K, E13K and E13A Pn3a analogues. The nature of the residue at position 10 and 13 did not have a large impact on activity, as E10K (IC_{50} 1 nM), E13K (IC_{50} 2 nM) and E13A (IC_{50} 12 nM) had only 4-fold and 2-fold improvement, and 3-fold decrease in potency at Nav1.7, respectively (**Fig. 2D, Table 1**).

We also generated D12T and D14K based on similarity to Hm1a and ProTx-II, respectively, but found that these analogues did not adopt the native fold (**Fig. S1**) and were inactive at Nav1.7 up to 1 μ M (**Fig. 2D, Table 1**). The NMR solution structure of Pn3a (PDB 5T4R) suggests a possible salt bridge between D12 and R23 as well as hydrogen bonds of D14 with the K11 side chain and the backbone amide hydrogens of E10 and K11 (**Fig. S3**), suggesting that the side chains of D12 and D14 are important for the stability of the correct fold. This might explain the low synthetic folding yields of Hm1a and Hm1b, which required regioselective disulfide-bond formation to produce useful quantities²⁹. In contrast, Pn3a can be synthesized using a non-selective approach with reasonable yield.

In summary, six mutations (D1K, D8N, D8K, E10K, E13K and K24R) were identified that resulted in improved potency at hNav1.7. Furthermore, four amino acids (Y4, K22, K24 and W30) were shown to be an important part of the pharmacophore of Pn3a for potent Nav1.7 inhibition and three residues (D12, D14 and Y27) were identified as important for folding of Pn3a into its native and active inhibitor cysteine knot (ICK) structure.

1.6 Selectivity of Pn3a analogues with improved potency at Nav1.7

We next estimated the Nav1.1-1.8 selectivity of the Pn3a analogues with improved potency at Nav1.7 using a high-throughput fluorescence-based assay, to assess the impact of these mutations on the potency at other Nav channel isoforms. The rank order of selectivity for Nav1.7 (Nav1.7 > Nav1.2 > Nav1.1 > Nav1.4 > Nav1.3 > Nav1.8 ≥ Nav1.5 = Nav1.6) (see **Table S1** for full selectivity values) was maintained for all analogues except E10K and E13K, which gained potency at Nav1.6 (**Fig 3A, Table S1**).

In the peripheral nervous system, Nav1.6 expression is highly localized to the nodes of Ranvier, where it contributes to the saltatory conduction of action potentials on both myelinated sensory and motor neurons³⁶. This makes Nav1.6 a major off-target for peripherally restricted Nav channel blockers, as pharmacological inhibition of Nav1.6 will likely cause intolerable motor adverse effects^{37, 38}. We therefore assessed the potency of Pn3a analogues with improved potency at Nav1.7 at Nav1.6 using patch-clamp electrophysiology. Wild-type Pn3a inhibits Nav1.6 with an IC₅₀ of 129 nM, making it at least 100-fold selective for Nav1.7 over Nav1.6²¹. This selectivity window was maintained for D1K, D8N and K24R, which had Nav1.6 IC₅₀ values of 102 nM, 25 nM and 137 nM, respectively (**Fig. 3B**). D8K displayed an intermediate selectivity (34-fold) over Nav1.6 with an IC₅₀ of 10 nM. Relative to Nav1.7, E10K and E13K gained the most potency at Nav1.6, with IC₅₀ values of 12 nM and 30 nM, respectively, indicating that E10 and E13 residues are important in Pn3a for imparting selectivity over Nav1.6 (**Fig. 3B**). This suggests that residues on the hydrophilic face, opposite to the hydrophobic “active” surface, can change peptide pharmacodynamics and should not be disregarded when attempting to engineer potent and selective ICK peptides. The changes in selectivity for Nav1.6 determined using electrophysiology

matched those estimated from the fluorescence-based assays, validating this high-throughput approach as a method for estimating Nav selectivity.

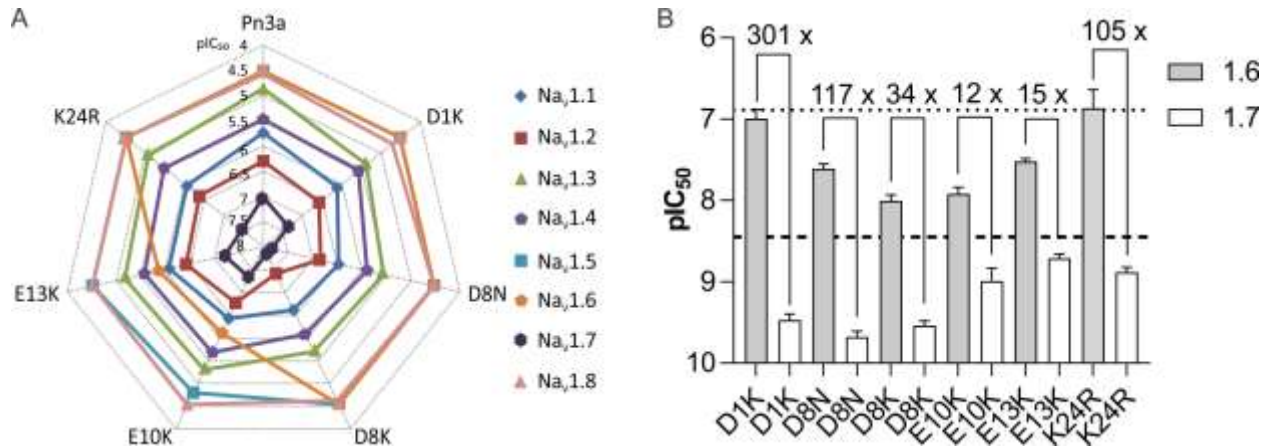


Figure 3: Nav_v1.1-1.8 selectivity of Pn3a analogues with improved potency at Nav_v1.7. **(A)** Potency at hNav_v1.1-1.8 represented on a radar plot assessed using fluorescence-based assays with membrane potential dye. Data is presented as the pIC₅₀ averaged from 3 independent replicates (each with 3 identical wells per treatment) **(B)** Comparative potency of select Pn3a analogues at hNav_v1.6 and hNav_v1.7 assessed by whole-cell patch-clamp experiments. Numbers above bars indicate fold selectivity for Nav_v1.7 over Nav_v1.6. Dashed and dotted lines indicate potencies of wild-type Pn3a at Nav_v1.7 and Nav_v1.6, respectively (values for Nav_v1.6 as previously reported²¹). Data are presented as mean ± SEM; n = 4–7 cells).

1.7 Pn3a analogues effectively engage Nav1.7 in vivo

We next assessed Nav_v1.7 target engagement of Pn3a analogues following local and systemic administration using a previously validated mouse model of Nav_v1.7-mediated pain induced by intraplantar injection of the scorpion toxin OD1³⁹. E10K and E13K were not tested *in vivo* due to their small selectivity window over Nav_v1.6 (12–15-fold). Intraplantar injection of wild-type Pn3a (1 μM) partially reduced OD1-induced spontaneous pain behaviors (Control: 89 ± 6 flinches; Pn3a: 42 ± 3 flinches; **Fig. 4A**), confirming Nav_v1.7 target engagement and inhibition at peripheral nerve terminals *in vivo*. At the same concentration, D1K, D8N, D8K, and K24R almost completely abolished OD1-induced pain behaviors, consistent with their increased potency at Nav_v1.7 *in vitro* (D1K: 2 ± 1 flinches; D8N: 6 ± 2 flinches; D8K: 2 ± 1 flinches; K24R: 15 ± 4 flinches; **Fig. 4A**).

We therefore next assessed systemic antinociceptive activity of the active Pn3a analogues. Following intraperitoneal injection, Pn3a D1K, D8N, D8K and K24 (1 mg/kg) all significantly attenuated OD1-induced pain behaviors (Control: 119 ± 7 flinches, Pn3a: 37 ± 7 flinches; D1K: 28 ± 13 flinches; D8N: 6 ± 2 flinches; D8K: 21 ± 11 flinches; K24R: 74 ± 6 flinches; **Fig. 4B**), and D8N stood out as significantly more effective compared to Pn3a ($P < 0.05$, unpaired t-test).

Despite being more potent than native Pn3a *in vitro*, K24R performed worse following systemic administration. A disconnection between *in vitro* potency and systemic *in vivo* efficacy is a common problem in the development of analgesic Nav1.7 blockers (including small molecules and peptides), suggesting insufficient free plasma concentration or inaccessibility of relevant receptor sites⁶. Another possible explanation may be the modest shift of the voltage-dependence of activation by K24R, which only caused a $\Delta +11.0$ mV (from -22.62 mV to -11.67 mV) shift compared with a 21.3 mV shift for Pn3a (**Fig. S4**). In summary, these results highlight D8N as the most potent Pn3a analogue *in vivo* after systemic administration and therefore a promising analgesic lead compound for further assessment.

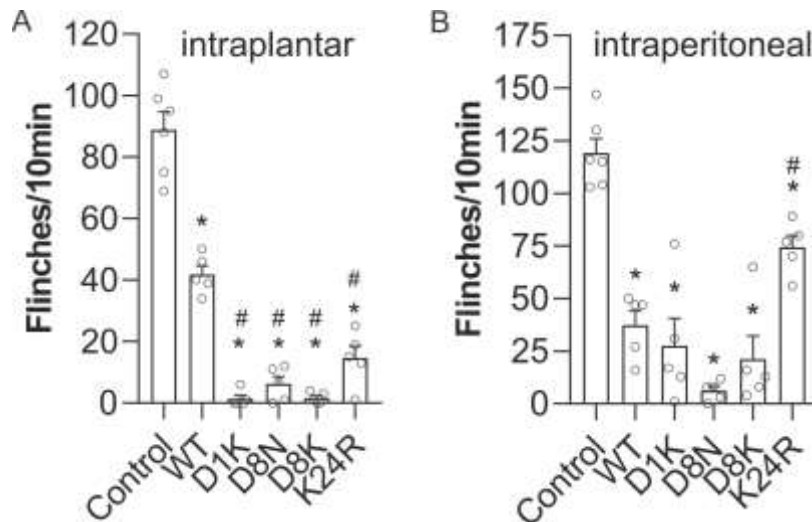


Figure 4. Comparative efficacy of Pn3a and analogues in a mouse model of Nav1.7 mediated pain. **(A)** Local injection of Pn3a (WT) and analogues (i.pl. 1 μ M) reverses spontaneous pain behaviors induced by intraplantar injection of the Nav1.7 activator OD1 in mice; n = 5–6 per group. **(B)** Systemic administration of Pn3a (WT) and analogues (i.p. 1 mg/kg) reverses spontaneous pain behaviors induced by intraplantar injection of the Nav1.7 activator OD1 in mice; n = 5–6 per group. Data are presented as mean \pm SEM. Statistical significance was determined using one-way ANOVA with Dunnett’s post-test; * P < 0.05 compared to control, # P < 0.05 compared to native Pn3a (WT).

1.8 Pn3a[D8N] maintains selectivity for Nav1.7 and is a potent analgesic

Since Pn3a[D8N] showed improved potency at Nav1.7 and was significantly more analgesic *in vivo* than wild-type Pn3a after systemic administration, we next sought to confirm selectivity over other Nav subtypes using patch-clamp electrophysiology. Pn3a[D8N] exhibited similarly increased potencies across all of the Nav subtypes when compared to native Pn3a, maintaining at least 100-fold selectivity over the major off-targets Nav1.4, Nav1.5 and Nav1.6 (**Fig. 5A, Table 2**). This increase in potency correlates with an increase in lipid membrane interactions (see Supporting Information and **Fig. S5 and Table S2**) suggesting that the removal of the negatively charged D8 residue drives overall potency via improved membrane affinity rather than by direct channel interactions. Indeed, membrane affinity seems to play an important role in the activity of Nav blockers⁴⁰ and has been well studied for e.g. ProTx-II and HwTx-IV^{31, 33}. The mechanism of

Nav1.7 channel block by Pn3a[D8N] remained the same as for native Pn3a, with Pn3a[D8N] causing a large depolarizing shift in the voltage-dependence of activation ($\Delta +22.4$ mV), consistent with overlapping VSDII interactions (**Fig. 5B, C and S4**). This closely matches the previously reported shift of $\Delta +21.3$ mV of wild-type Pn3a²¹ and further suggests that the D8N mutation does not change direct interactions of Pn3a with Nav1.7 channels.

We next determined analgesic efficacy of systemic Pn3a[D8N] doses using the OD1 model. Intraperitoneal administration of Pn3a[D8N] dose-dependently reduced OD1-induced flinching, with 1 mg/kg almost completely abolishing all spontaneous pain behaviors (Control: 102 ± 3 ; D8N 0.3 mg/kg: 105 ± 18 ; D8N 0.6 mg/kg: 34 ± 11 ; D8N 1 mg/kg: 6 ± 2 ; **Fig. 4B and 5D**). We therefore took this dose forward into a clinically relevant model of post-surgical pain, in which Nav1.7 inhibition was previously shown to be analgesic²². Pn3a[D8N] (1 mg/kg) significantly attenuated surgically induced mechanical allodynia (Control: 0.9 ± 0.1 g; Pn3a[D8N] 1 mg/kg: 2.5 ± 0.3 g), while native Pn3a at the same dose had no significant effect (Control: 0.9 ± 0.1 g; Pn3a 1 mg/kg: 1.2 ± 0.3 g), consistent with Pn3a[D8N] being more potent than native Pn3a at Nav1.7 (**Fig. 5E**). Analgesic doses of Pn3a (3 mg/kg) and Pn3a[D8N] (1 mg/kg) had no significant motor adverse effect as measured with the parallel rod floor test (ataxia index; control: 4.6 ± 0.8 ; Pn3a, 7.0 ± 1.5 ; Pn3a[D8N]: 6.9 ± 1.3 ; $P > 0.05$, one-way ANOVA), confirming the analgesic effects were not due to motor impairment. Increasing the dose of Pn3a[D8N] to 3 mg/kg resulted in full reversal of mechanical allodynia with withdrawal thresholds indifferent from healthy mice ($P > 0.05$, one-way ANOVA; **Fig. 5E**), while still not causing motor impairments (ataxia index: 4.9 ± 1.5 ; $P > 0.05$ vs control, one-way ANOVA). The anti-nociceptive activity of systemically administered Pn3a[D8N] (3 mg/kg, i.p.) persisted for at least 1 h (**Fig. 5F**), consistent with an expected short half-life due to rapid renal clearance that is typical for small globular peptides^{41, 42}.

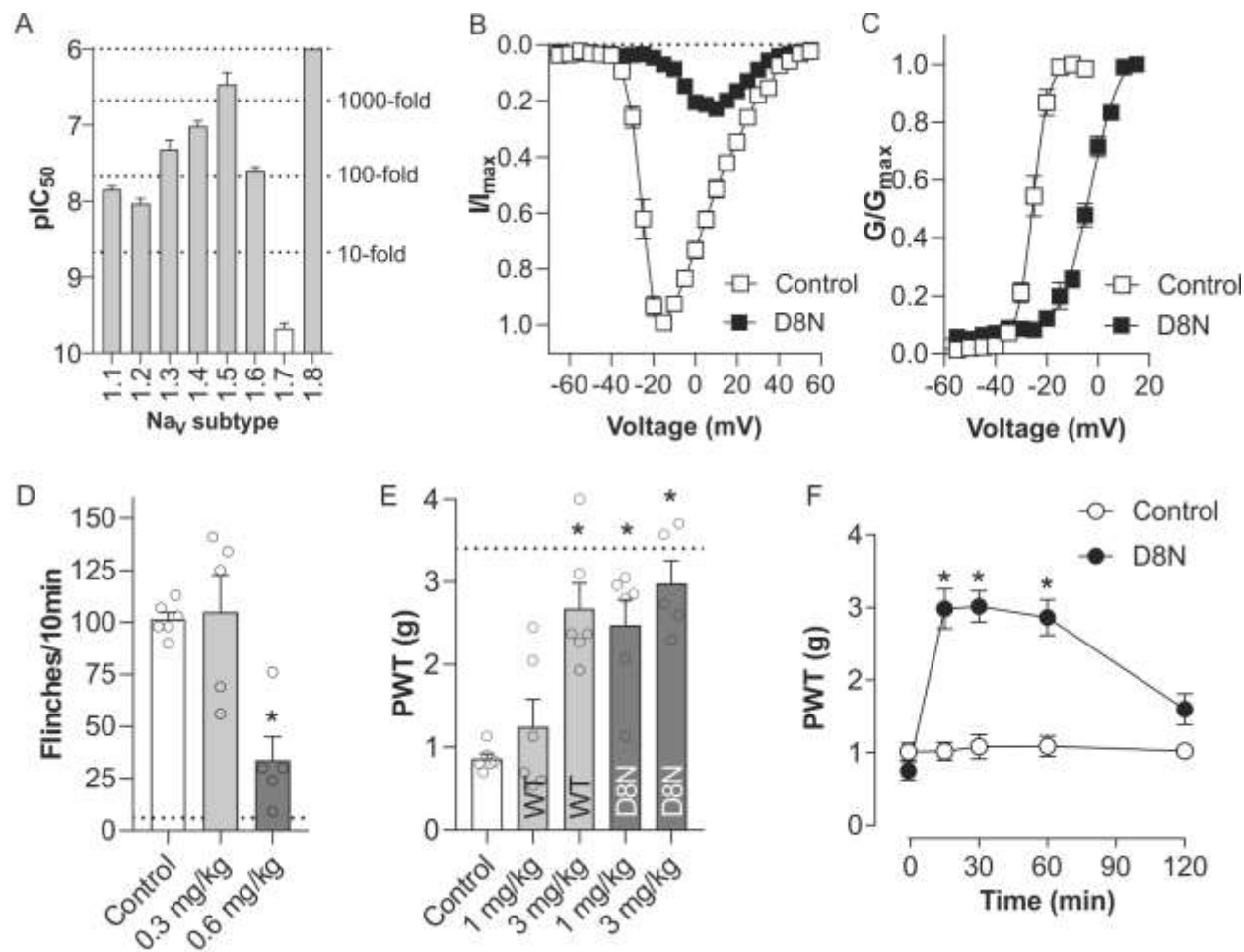


Figure 5. Pharmacological characterization of Pn3a[D8N] with improved potency at Nav1.7 (A) Comparative potency of [D8N]Pn3a at hNav1.1-1.8 assessed by whole-cell patch-clamp experiments. [D8N]Pn3a most potently inhibited Nav1.7 (IC_{50} 0.21 nM), with >40-fold selectivity over Nav1.1 and Nav1.2, >100-fold selectivity over Nav1.3, Nav1.4 and Nav1.6, and >1000-fold selectivity over Nav1.5 and Nav1.8. (B) Current-voltage (IV) relationship before and after addition of Pn3a[D8N] (100 nM) at Nav1.7. (C) Conductance-voltage (GV) relationship before and after addition of Pn3a[D8N] (100 nM) at Nav1.7. Pn3a[D8N] shifted the voltage-dependence of activation by +22.4 mV. Data are presented as mean \pm SEM, with $n = 3-7$ cells per data point. (D) Pn3a[D8N] (i.p.) dose-dependently reversed spontaneous pain behaviors induced by intraplantar injection of the Nav1.7 activator OD1 in mice; $n = 5-6$ per group. Dotted line represents pain behaviors after i.p. injection of 1 mg/kg D8N. (E) Comparative efficacy of Pn3a (1 and 3 mg/kg i.p.) and Pn3a[D8N] (1 and 3 mg/kg i.p.) on postsurgical pain-induced mechanical allodynia in mice; $n = 5-6$ per group. Dotted line represents mechanical thresholds of naïve mice. (F) Time course of reversal of postsurgical pain-induced mechanical allodynia by Pn3a[D8N] (3 mg/kg i.p.); $n = 5$ per group. Data are presented as mean \pm SEM. Statistical significance was determined using one-way or two-way ANOVA with Dunnett's post-test as appropriate; * $P < 0.05$ compared to control.

Table 2: Pn3a[D8N] and Pn3a potency at Nav1.1-1.8 and selectivity for Nav1.7. Data is presented as mean IC₅₀ assessed by whole-cell patch-clamp experiments. Values for wild-type Pn3a as previously reported²¹. The fold selectivity for Nav1.7 over each other isoform was calculated as IC₅₀ (Nav1.X)/IC₅₀ (Nav1.7)

Nav subtype	Pn3a[D8N]		Pn3a	
	IC ₅₀ [nM]	Nav1.7 selectivity	IC ₅₀ [nM]	Nav1.7 selectivity
1.1	14	67	37	41
1.2	9	43	124	138
1.3	48	229	210	233
1.4	97	462	144	160
1.5	343	1633	800	889
1.6	25	119	129	143
1.7	0.21	1	0.9	1
1.8	>1000	>4762	>1000	>1111

1.9 Molecular model of the interaction between Pn3a and Nav1.7 VSDII in the “down” state

Recent advances in cryo-EM technology have made it possible to obtain high resolution structures of human Nav1.7 channels or chimeric hNav1.7(VSDII)-NavAb channels in complex with gating-modifier toxins bound to the voltage-sensing domains of the channel^{12, 43}. Particularly interesting was the high-resolution visualization of ProTx-II bound to VSDII in the putative down/closed state, the state that is preferentially bound and blocked by gating modifying channel inhibitors like Pn3a¹². Since the binding site of Pn3a overlaps with ProTx-II (**Fig. 1B**) and Pn3a shows several similarities in its pharmacophore compared to ProTx-II (**Fig. 1D**), we used this cryo-EM structure to model the binding of Pn3a to the “down” state of VSDII of the hNav1.7/NavAB chimera (**Fig. 6A**). Our model is consistent with experimentally obtained data described in previous sections and places both basic residues K22 and K24 in Pn3a in close proximity of D816 and E818, respectively, where they likely form ionic and/or hydrogen bonds with these negatively charged S3-S4 loop residues (**Fig. 6B**). These interactions would likely interfere with S4 gating charge movement by neutralizing necessary acidic side chains or even by repulsing forces of these positive charges, to

interfere with channel opening. Consistent with our experimental data showing a slight loss of activity for K22R, this model also suggests that the bulkier and slightly longer arginine may clash with the D816 residue, while an arginine at position 24 would permit closer engagement with E818. Future studies systematically exploring a variety of amino acids, including unnatural amino acids like homo- and nor-arginines, or channel mutagenesis, may provide additional experimental evidence supporting this explanation for the observed pharmacological activity of the K22R and K24R analogues.

Furthermore, modeling of Pn3a to the VSDII of Nav1.7 suggest that the side chains of the hydrophobic residues M5, F6, Y27, W30 and F34 in Pn3a are embedded in the membrane, with possible interactions between M5, F6 and W30 in Pn3a and the Nav1.7 specific F813 side chain, supporting the idea that direct channel interactions contribute to the loss of potency we observed *in vitro* in the corresponding Nav1.7 mutant (**Fig. 6A**). Interestingly, ProTx-II shows only slight interaction with F813¹², however, this residue seems crucial for stabilization of the S3 helix which in turn orients the S3-S4 loop residues to permit close interactions with ProTx-II. In comparison, the glycine residue in Nav1.5 (corresponding to F813 in hNav1.7) seems to result in a less polar surface in the S3-S4 loop binding region, providing an explanation for ProTx-II having lower affinity for Nav1.5¹². W24 in ProTx-II is one of the few residues making intimate contacts with Nav1.7¹² and the molecular models suggest that Pn3a M25 and Y27 play a similar role, making hydrophobic contacts with the receptor L770 and L812 and the side chain Y27 establishing a hydrogen bond with the backbone carbonyl of L812. Additionally, our model indicates hydrophobic contacts between VSDII L814 and Pn3a W30 and F34 (**Fig. 6A**). The side chain of Pn3a W30 therefore potentially interacts with the first two residues of the S3-S4 segments as well as the membrane, and this central role is supported by the loss of inhibition measured

experimentally when W30 is mutated to alanine (**Table 1**). Future studies on further Nav1.7 mutant channels including D816, E818, L770, L812 and L814 mutants will be necessary to confirm the roles of these residues in Pn3a activity at Nav1.7. Similarly, mutagenesis experiments to introduce Nav1.7-like residues into other Nav1.X channels could be used to confirm importance of individual channel residues in potency and selectivity of Pn3a.

According to the model, D8 is positioned over the head groups of the lipid membrane, which presumably contains negatively charged moieties^{44, 45}. Our data suggests that a negative charge at position 8 is poorly tolerated near the lipid headgroups, whereas an uncharged polar residue or a basic residue with a long sidechain is preferred and indeed this aligns with our experimental findings that D8N and D8K show improved membrane binding properties and an increased potency at Nav1.7 (**Fig. 6C and S5**). Similarly, the negative aspartic acid at position 1 of the flexible N-terminus may be affected by repulsive long range electrostatic interactions of negative charges within the membrane, while the N-terminal lysine of D1K would experience attractive long range electrostatic effects resulting in higher affinity to the channel-membrane complex as confirmed by the improved potency of D1K at Nav1.7.

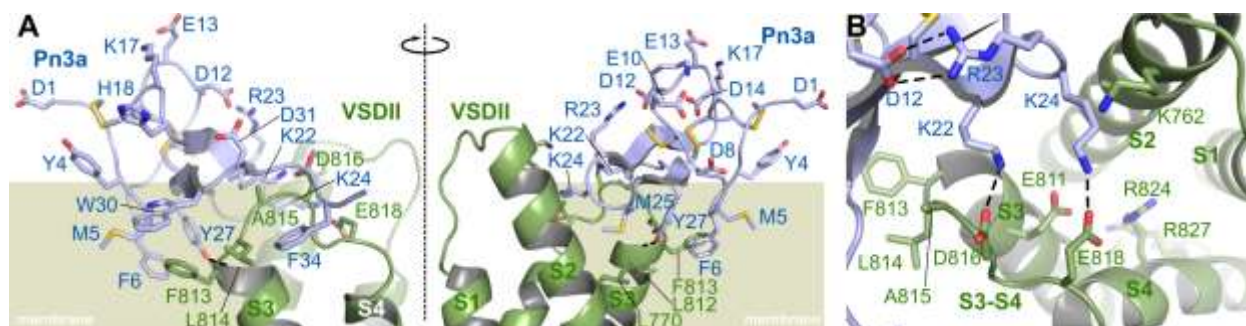


Figure 6: Molecular model of the interaction between Pn3a and Nav1.7 VSDII “down” state. **(A)** Two cross-membrane views (180 degrees rotated) of the interaction between the VSDII of Nav1.7 (green) and Pn3a (blue). The position of the lipid bilayer is indicated in olive. **(B)** View parallel to the membrane

showing the interaction of K22 and K24 with counter charges D816 and E818 in the S3-S4 segment. Only the side chains of selected residues are represented as sticks to increase readability. Hydrogen-bonds that are discussed in the text are indicated by dashed lines. The VSDII is made of four α -helices noted S1 to S4. The molecular models were generated by homology using three templates: the cryo-EM structure of hNav1.7 VSDII-NavAB chimera in complex with ProTx-II (PDB 6n4r), the cryo-EM structure of hNav1.7 (PDB 6j8h) and the NMR solution structure of Pn3a (PDB 5t4r).

In summary, our structure-activity-relationship study of the family 2 peptide Pn3a identifies residues necessary for potent and selective inhibition of Nav1.7. Despite limited sequence similarity to ProTx-II, Pn3a binds to an overlapping site on VSDII, with the large interaction surface of the peptide seeming to drive selectivity over other Nav subtypes. The Pn3a analogue Pn3a[D8N] was more potent *in vitro* and also displayed more potent analgesic activity *in vivo* in a target engagement model as well as a model of post-surgical pain.

2. Materials and Methods

2.1 Sequence alignment of Pn3a

Amino acid sequences of peptides were aligned using clustal omega and the UniProtKB database (<http://www.uniprot.org/>; entry IDs: Pn3a: P0DM12; SGTx1: P56855; Hm1a: P60992; Hm1b: P0DOC5; ProTx-II: P83476) and manually corrected for cysteine spacing.

2.2 Structural alignment of Pn3a

The 2D NMR solution structures of Pn3a (PDB 5T4R)²¹ and Hm1a (PDB 2N6O)²⁹ or ProTx-II (PDB 2N9T)³¹ were superimposed over the disulfide bonds, using the molecular graphics program PyMol.

2.3 Solid-phase peptide synthesis of Pn3a and Pn3a-analogues

Pn3a and analogues were synthesized using solid-phase peptide synthesis as described previously²². Briefly, synthesis was performed on a Symphony automated peptide synthesizer (Gyros Protein Technologies, Inc, Tucson, AZ), using Fmoc protocols. Peptides were released from the polystyrene resin and simultaneously deprotected, precipitated with ice-cold di-ethyl ether and HPLC purified. The linear peptides were folded in oxidation buffer containing a mix of oxidized and reduced glutathione for 48 h and then HPLC purified to obtain the final folded peptide products. The peptides were analyzed via electrospray ionization mass spectrometry using an API2000 system (Applied Biosystems, Foster City, CA, USA) to confirm matching calculated and measured masses (**Table S3**) and via analytical RP-HPLC using a Hypersil GOLD C18 column (2.1 × 100 mm, particle size 3 μm; Thermo Fisher Scientific, Waltham, MA, USA) on a Shimadzu LC20AT (Shimadzu Corporation, Kyoto, Japan) to confirm elution of clean, symmetrical peaks

(**Fig. S6**). The peptides were further analyzed for proper folding via 1D NMR (**Fig. S1**) and quantified using a Nanodrop spectrophotometer (Thermo Fisher Scientific, Scoresby, Australia).

2.4 NMR spectroscopy

To ensure that the Pn3a analogues displayed the same overall fold as native Pn3a, we performed one-dimensional ^1H nuclear magnetic resonance (NMR) spectroscopy on a Bruker Avance III 700 MHz NMR spectrometer equipped with a cryo-probe ⁴⁶. The samples were prepared at a concentration of 50 μM and dissolved in 95% H_2O /5% deuterium oxide (D_2O). To process the spectra, TopSpin 3.5 (Bruker) was used. Agreement of resonance positions in the NH region of Pn3a-analogues compared to that of the native (and biologically active) Pn3a were used to assess folding.

2.5 Generation of [F823G]Nav1.7 plasmid

The QuikChange II XL kit (Agilent Technologies, Santa Clara, CA, USA) was used for site-directed mutagenesis on murine *Scn9a* (encoding mNav1.7) containing plasmids (GenScript, Piscataway, NJ, USA; Accession number NM_001290674, transcript variant 1) according to the manufacturer's instructions to introduce a F823G mutation, equivalent to F813 in hNav1.7. The vector used was pcDNA3.1-Hygro(+) including CMV and SV40 promoters for mammalian expression and a Hygromycin B resistance gene. PCR and Sanger sequencing of the whole open-reading frame was performed to confirm presence of desired and absence of unwanted mutations.

2.6 Cell culture

Human embryonic kidney 293 (HEK293) cell lines stably expressing human Nav1.1-Nav1.8 channels (SB Drug Discovery, Glasgow, UK) were cultured in minimal essential medium eagle (MEM; Sigma-Aldrich; Castle Hill, NSW) containing 10% (v/v) fetal bovine serum (FBS; Assay

Matrix Pty Ltd), 2 mM L-glutamine and selection antibiotics as recommended by the manufacturer. Chinese hamster ovary (CHO) cells stably expressing human Nav1.8 in a tetracycline-inducible system (ChanTest, Cleveland, OH) were cultured in Ham's F-12 containing 10% (v/v) FBS and selection antibiotics as recommended by the manufacturer and hNav1.8 expression was induced by the addition of tetracycline (1 µg/ml) for 24 h at 27 °C. HEK293 cells stably expressing mNav1.7 or [F823G]mNav1.7 were generated by transfection with Lipofectamine 3000 (Thermo Fisher Scientific, Waltham, MA, USA) using 20 µg plasmid DNA and 30 µL Lipofectamine 3000, and selection of stable clonal cell lines with robust Nav currents using hygromycin B (100 µg/mL). Cells were grown in an incubator at 37 °C with 5% CO₂ and passaged every 3–4 days (at 70–80% confluency) using TrypLE Express (Thermo Fisher Scientific).

2.7 Whole-cell patch-clamp electrophysiology

To pharmacologically characterize Pn3a analogues, whole-cell voltage-clamp electrophysiology assays were performed on Nav1.1-Nav1.7 expressing HEK293 cells and Nav1.8 expressing CHO cells using the automated electrophysiology platform QPatch-16X (Sophion Bioscience, Ballerup, Denmark) as previously described ⁴⁷.

The extracellular solution contained in mM: NaCl 70 (140 mM for Nav1.1-1.3, Nav1.6 and mNav1.7/F823G), choline chloride 70 (0 mM for Nav1.1-1.3, Nav1.6 and mNav1.7/F823G), KCl 4, CaCl₂ 2, MgCl₂ 1, HEPES 10 and glucose 10; pH 7.4; osmolarity 305 mOsm. The intracellular solution contained in mM: CsF 140, EGTA 1 CsOH 5, HEPES 10 and NaCl 10; pH 7.3 (adjusted with CsOH); osmolarity 320 mOsm. Pn3a analogues were diluted in extracellular solution containing 0.05% bovine serum albumin (BSA). All compound effects were compared to solvent controls following 5 min of incubation.

Concentration-response curves were obtained by measuring the inhibition of peak current (I/I_{\max}) elicited by a 20 ms test pulse of -20 mV from a holding potential of -90 mV (at 0.05 Hz frequency), using increasing peptide concentrations (each incubated for 5 min after addition). To calculate IC_{50} values, a four-parameter Hill equation with variable Hill slope was fitted to the data using GraphPad Prism v7.00 (San Diego, CA, USA). Current-voltage (I-V) curves were generated before and after addition of peptide from a holding potential of -90 mV with a step pulse series (500 ms each, 5 mV increments), ranging from -110 mV to $+55$ mV. Conductance (G) at each voltage (V) was calculated with the equation $G = I/(V - V_{\text{rev}})$, (with V_{rev} = reversal potential) to obtain the conductance-voltage curves which were fitted with a Boltzmann equation with GraphPad Prism v7.00. Data are presented as the mean \pm standard error of the mean (SEM).

2.8 Fluorescence imaging plate reader (FLIPR) membrane potential assay

To assess the concentration-response relationship and Na_v -isoform selectivity of Pn3a-analogues on human $Na_v1.1$ - $Na_v1.8$ channel isoforms, fluorescence imaging plate reader (FLIPR) membrane potential assays were performed on a FLIPR^{TETRA} cellular screening system (Molecular Devices, Sunnyvale, CA, USA) as previously described⁴⁷. Freshly dissociated cells were seeded into clear-bottom black-walled 384-well imaging plates (Corning, NY, USA) at a density of $\sim 10,000$ cells/well. Growth media was removed from the wells after 48 h and the adherent, confluent cells loaded with 20 μ L/well red membrane potential dye (Molecular Devices) diluted in physiological salt solution (PSS) for 30 min at 37 °C, 5% CO_2 . PSS contained in mM: NaCl 140, glucose 11.5, KCl 5.9, $MgCl_2$ 1.4, NaH_2PO_4 1.2, $NaHCO_3$ 5, $CaCl_2$ 1.8 and HEPES 10; adjusted to pH 7.4. Pn3a-analogues were diluted in PSS containing 0.1% BSA and added to the Na_v channel expressing HEK293 cells using the FLIPR^{TETRA}. Cells were incubated for 5 min with peptides prior to addition of 20 μ M veratridine ($Na_v1.6$), 60 μ M veratridine ($Na_v1.1$ -1.5 and 1.7) or 150 μ M deltamethrin

(Nav1.8) for Nav channel stimulation. Changes in fluorescence intensity (excitation 515–545 nm; emission 565–625 nm), equivalent to changes in membrane potential, were measured with a cooled CCD camera. Reads were taken every 1 s for 10 s before (baseline values), 300 s after peptide addition and a further 300 s after addition of Nav channel activators. PSS containing 0.1% BSA was used as a negative control.

Raw fluorescence values were converted to response over baseline values and a negative control correction was performed using the FLIPR^{TETRA} software ScreenWorks 3.2.0.14 (Molecular Devices). The computed area under the curve (AUC) values over 300 s after activator addition were plotted and inhibitory peptide effects analyzed using GraphPad Prism v7.00. To calculate IC₅₀ values, a four-parameter Hill equation with variable Hill slope was fitted to the data. All experiments were performed in triplicate for each treatment (three wells per condition) and the assay was performed on at least three separate occasions.

2.9 Analgesic efficacy of Pn3a and analogues *in vivo*

All *in vivo* experiments in mice were performed in accordance with the *International Association for the Study of Pain Guidelines for the Use of Animals in Research* and the *Australian Code of Practice for the Care and Use of Animals for Scientific Purposes*, 8th edition (2013). Ethical approval for experiments involving animals was obtained from the University of Queensland animal ethics committee. The behavioral experiments were conducted using male C57BL/6J mice (aged 6–9 weeks; sourced from *Animal Resources Centre*, WA, Australia), housed in groups of 3–4 per cage under 12 h light-dark cycles, with access to standard rodent chow and water *ad libitum*. A blinded observer (unaware of the treatment received by each animal) performed all measurements.

To determine *in vivo* target engagement, efficacy was assessed in the mouse model of OD1-induced spontaneous pain as previously described³⁹. For local treatments, vehicle (0.1% BSA in saline) or Pn3a-analogues (1 μ M) were co-administered with the α -scorpion toxin OD1 (300 nM) via shallow subdermal intraplantar (i.pl.) injection (40 μ L) into the right hind paw. For systemic treatments, vehicle or peptides were administered via intraperitoneal (i.p.) injection (10 μ L/g; 0.3–3 mg/kg) 10 min before injection of OD1 (300 nM; 40 μ L i.pl.). After injection of OD1, mice were transferred to transparent enclosures and videotaped for up to 30 min from below. Spontaneous nocifensive behaviors including licking, shaking, lifting or flinching of the injected paw was counted by a blinded observer from the video recordings. All data are expressed as mean \pm SEM. Statistical significance compared to vehicle controls was determined in GraphPad Prism v7.00 using one-way ANOVA with Dunnett's multiple comparison test.

An *in vivo* mouse model of post-surgical pain was used to assess the analgesic activity of Pn3a and Pn3a[D8N] as described previously²². Briefly, during anesthesia, an incision was made through the plantar skin, fascia and underlying *flexor digitorum brevis* muscle of the right hind paw. To simulate tissue retraction, the muscle was carefully elevated, leaving muscle origin and insertion intact. The wound was closed after hemostasis with two simple interrupted sutures and treated with 5% povidone-iodine solution. The mice were allowed to recover in their home cages until behavioral experiments. After 24 h of recovery, mice were systemically treated with vehicle (0.1% BSA in saline) or peptides, administered via i.p. injection (10 μ L/g; 1–3 mg/kg) 10 min before measurement of mechanical allodynia. Paw withdrawal thresholds to mechanical stimulation were determined 24 h post-surgery using an electronic von Frey apparatus (Mouse-Met Electronic von Frey, Topcat Metrology Ltd, Little Downham, United Kingdom) as previously described²².

2.10 In vivo locomotor performance test

Motor impairment 20 min after peptide administration was measured using the Parallel Rod Floor apparatus (Stoelting Co, Wood Dale, IL) and data analyzed using the ANY-Maze software (Stoelting Co) as described previously³⁹. The number of foot slips within one minute was divided by the distance travelled to obtain the ataxia index.

2.11 Molecular docking of Pn3a at hNav1.7

A molecular model of the interaction between Pn3a and Nav1.7 VSDII was proposed by comparative modeling computed using Modeller 9v20⁴⁸ and as templates the NMR solution structure of Pn3a (PDB 5T4R²¹), the cryo-EM structure of the hNav1.7 (in complex with Huwentoxin-IV; PDB 6J8H; resolution 3.2 Å⁴³) and the cryo-EM structure of hNav1.7-VSDII/NavAB chimera in complex with ProTx-II (PDB 6N4R¹²). The six C α of the cysteine residues of experimental structure of Pn3a and ProTx-II align with 0.5 Å root-mean-square deviation, indicating the scaffold of these two peptides are highly similar. Beside the cysteine framework, the conformation of the loops 1 and 3 of Pn3a and ProTx-II are similar and were used as anchor point to dock Pn3a on Nav1.7 VSDII using the homology modelling approach. A hundred models were built using Modeller, and the model displaying the lowest DOPE score⁴⁹ was selected and then energy minimized using Amber 18 and the FF14SB force field⁵⁰. The Molprobit⁵⁰ score of the tmodels is 1.36 (98th percentile), suggesting that it has very good quality.

2.12 Statistical analysis

Data and statistical analysis was performed using GraphPad Prism v7.00 (San Diego, CA, USA). Statistical significance was determined as a p -value < 0.05 (with $*p < 0.05$; $**p < 0.01$; $***p < 0.001$; $****p < 0.0001$) and was calculated using unpaired t -tests (two-tailed), one-way analysis

of variance (ANOVA) with either Tukey's multiple comparison test or Dunnett's multiple comparison test or two-way ANOVA with Sidak's multiple comparison test as appropriate, unless otherwise stated. Data are presented as the mean \pm standard error of the mean (SEM) of at least three individual measurements.

Supporting Information

Supplementary materials and methods (surface plasmon resonance); supplementary results and discussion (membrane binding properties of Pn3a and analogues); supplementary figures S1 to S6; supplementary tables S1 to S3; SI references

Acknowledgements

The authors thank the University of Queensland Protein Expression Facility for technical help with site-directed mutagenesis and plasmid sequencing.

A.M. is supported by an Australian Government Research Training Program Scholarship. A.J.A. and H.S. were supported by a University of Queensland International Postgraduate Scholarship. This work was funded by the Australian National Health and Medical Research Council (NMHRC) through a NHMRC Research Fellowship (P.F.A), a NHMRC Career Development Fellowship (APP1162503) awarded to I.V., a NHMRC Early Career Fellowship (APP1139961) awarded to J.D. and Development (APP1137011, I.V.) and Project Grants (APP1125766, I.V.; APP1162597, M.M. and APP1080405, C.I.S.). C.I.S. is an Australian Research Council (ARC) Future Fellow (FT160100055).

Author contributions

A.M., J.R.D. and I.V. conceived the study and designed experiments. A.M., H.S., A.J.A. and J.R.D. conducted experiments and analyzed data. Q.K. performed molecular docking. C.I.S., Z.D., P.F.A. and M.M. provided reagents. A.M. and I.V. wrote the manuscript with input from all authors.

References

- [1] Gan, T. J., Habib, A. S., Miller, T. E., White, W., and Apfelbaum, J. L. (2014) Incidence, patient satisfaction, and perceptions of post-surgical pain: results from a US national survey, *Curr Med Res Opin* 30, 149-160. DOI: 10.1185/03007995.2013.860019
- [2] Cox, J. J., Reimann, F., Nicholas, A. K., Thornton, G., Roberts, E., Springell, K., Karbani, G., Jafri, H., Mannan, J., Raashid, Y., Al-Gazali, L., Hamamy, H., Valente, E. M., Gorman, S., Williams, R., McHale, D. P., Wood, J. N., Gribble, F. M., and Woods, C. G. (2006) An SCN9A channelopathy causes congenital inability to experience pain, *Nature* 444, 894-898. DOI: 10.1038/nature05413
- [3] Fertleman, C. R., Baker, M. D., Parker, K. A., Moffatt, S., Elmslie, F. V., Abrahamsen, B., Ostman, J., Klugbauer, N., Wood, J. N., Gardiner, R. M., and Rees, M. (2006) SCN9A mutations in paroxysmal extreme pain disorder: allelic variants underlie distinct channel defects and phenotypes, *Neuron* 52, 767-774. DOI: 10.1016/j.neuron.2006.10.006
- [4] Yang, Y., Wang, Y., Li, S., Xu, Z., Li, H., Ma, L., Fan, J., Bu, D., Liu, B., Fan, Z., Wu, G., Jin, J., Ding, B., Zhu, X., and Shen, Y. (2004) Mutations in SCN9A, encoding a sodium channel alpha subunit, in patients with primary erythralgia, *J Med Genet* 41, 171-174. DOI: 10.1136/jmg.2003.012153
- [5] Faber, C. G., Hoeijmakers, J. G., Ahn, H. S., Cheng, X., Han, C., Choi, J. S., Estacion, M., Lauria, G., Vanhoutte, E. K., Gerrits, M. M., Dib-Hajj, S., Drenth, J. P., Waxman, S. G., and Merkies, I. S. (2012) Gain of function Nav1.7 mutations in idiopathic small fiber neuropathy, *Annals of neurology* 71, 26-39. DOI: 10.1002/ana.22485
- [6] Vetter, I., Deus, J. R., Mueller, A., Israel, M. R., Starobova, H., Zhang, A., Rash, L. D., and Mobli, M. (2017) Nav1.7 as a pain target - From gene to pharmacology, *Pharmacol Ther* 172, 73-100. DOI: 10.1016/j.pharmthera.2016.11.015
- [7] McKerrall, S. J., and Sutherlin, D. P. (2018) Nav1.7 inhibitors for the treatment of chronic pain, *Bioorganic & medicinal chemistry letters* 28, 3141-3149. DOI: 10.1016/j.bmcl.2018.08.007

- [8] Kingwell, K. (2019) Nav1.7 withholds its pain potential, *Nature reviews. Drug discovery*. DOI: 10.1038/d41573-019-00065-0
- [9] Mobli, M., Undheim, E. A. B., and Rash, L. D. (2017) Chapter Seven - Modulation of ion channels by cysteine-rich peptides: From sequence to structure, In *Advances in Pharmacology* (Geraghty, D. P., and Rash, L. D., Eds.), pp 199-223, Academic Press.
- [10] Gilchrist, J., Olivera, B. M., and Bosmans, F. (2014) Animal toxins influence voltage-gated sodium channel function, *Handbook of experimental pharmacology* 221, 203-229. DOI: 10.1007/978-3-642-41588-3_10
- [11] Deuis, J. R., Mueller, A., Israel, M. R., and Vetter, I. (2017) The pharmacology of voltage-gated sodium channel activators, *Neuropharmacology* 127, 87-108. DOI: 10.1016/j.neuropharm.2017.04.014
- [12] Xu, H., Li, T., Rohou, A., Arthur, C. P., Tzakoniati, F., Wong, E., Estevez, A., Kugel, C., Franke, Y., Chen, J., Ciferri, C., Hackos, D. H., Koth, C. M., and Payandeh, J. (2019) Structural basis of Nav1.7 inhibition by a gating-modifier spider toxin, *Cell* 176, 702-715.e714. DOI: 10.1016/j.cell.2018.12.018
- [13] Ahern, C. A., Payandeh, J., Bosmans, F., and Chanda, B. (2016) The hitchhiker's guide to the voltage-gated sodium channel galaxy, *J Gen Physiol* 147, 1-24. DOI: 10.1085/jgp.201511492
- [14] Ahuja, S., Mukund, S., Deng, L., Khakh, K., Chang, E., Ho, H., Shriver, S., Young, C., Lin, S., Johnson, J. P., Jr., Wu, P., Li, J., Coons, M., Tam, C., Brillantes, B., Sampang, H., Mortara, K., Bowman, K. K., Clark, K. R., Estevez, A., Xie, Z., Verschoof, H., Grimwood, M., Dehnhardt, C., Andrez, J. C., Focken, T., Sutherlin, D. P., Safina, B. S., Starovasnik, M. A., Ortwine, D. F., Franke, Y., Cohen, C. J., Hackos, D. H., Koth, C. M., and Payandeh, J. (2015) Structural basis of Nav1.7 inhibition by an isoform-selective small-molecule antagonist, *Science* 350, aac5464. DOI: 10.1126/science.aac5464

- [15] Israel, M. R., Tay, B., Deuis, J. R., and Vetter, I. (2017) Chapter Three - Sodium channels and venom peptide pharmacology, In *Advances in Pharmacology* (Geraghty, D. P., and Rash, L. D., Eds.), pp 67-116, Academic Press.
- [16] Dongol, Y., Caldas Cardoso, F., and Lewis, R. J. (2019) Spider knottin pharmacology at voltage-gated sodium channels and their potential to modulate pain pathways, *Toxins 11*, 626.
- [17] Cardoso, F. C., and Lewis, R. J. (2019) Structure-function and therapeutic potential of spider venom-derived cysteine knot peptides targeting sodium channels, *Front Pharmacol 10*, 366. DOI: 10.3389/fphar.2019.00366
- [18] Schmalhofer, W. A., Calhoun, J., Burrows, R., Bailey, T., Kohler, M. G., Weinglass, A. B., Kaczorowski, G. J., Garcia, M. L., Koltzenburg, M., and Priest, B. T. (2008) ProTx-II, a selective inhibitor of Nav1.7 sodium channels, blocks action potential propagation in nociceptors, *Mol Pharmacol 74*, 1476-1484. DOI: 10.1124/mol.108.047670
- [19] Wu, B., Murray, J. K., Andrews, K. L., Sham, K., Long, J., Aral, J., Ligutti, J., Amagasu, S., Liu, D., Zou, A., Min, X., Wang, Z., Ilch, C. P., Kornecook, T. J., Lin, M. J., Be, X., Miranda, L. P., Moyer, B. D., and Biswas, K. (2018) Discovery of tarantula venom-derived Nav1.7-inhibitory JzTx-V peptide 5-Br-Trp24 analogue AM-6120 with systemic block of histamine-induced pruritis, *J Med Chem 61*, 9500-9512. DOI: 10.1021/acs.jmedchem.8b00736
- [20] Murray, J. K., Ligutti, J., Liu, D., Zou, A., Poppe, L., Li, H., Andrews, K. L., Moyer, B. D., McDonough, S. I., Favreau, P., Stocklin, R., and Miranda, L. P. (2015) Engineering potent and selective analogues of GpTx-1, a tarantula venom peptide antagonist of the Nav1.7 sodium channel, *J Med Chem 58*, 2299-2314. DOI: 10.1021/jm501765v
- [21] Deuis, J. R., Dekan, Z., Wingerd, J. S., Smith, J. J., Munasinghe, N. R., Bholra, R. F., Imlach, W. L., Herzig, V., Armstrong, D. A., Rosengren, K. J., Bosmans, F., Waxman, S. G., Dib-Hajj, S. D., Escoubas, P., Minett, M. S., Christie, M. J., King, G. F., Alewood, P. F., Lewis, R. J., Wood, J. N., and Vetter, I. (2017) Pharmacological characterisation of the highly Nav1.7 selective spider venom peptide Pn3a, *Sci Rep 7*, 40883. DOI: 10.1038/srep40883

- [22] Mueller, A., Starobova, H., Morgan, M., Dekan, Z., Cheneval, O., Schroeder, C. I., Alewood, P. F., Deuis, J. R., and Vetter, I. (2019) Antiallodynic effects of the selective Nav1.7 inhibitor Pn3a in a mouse model of acute postsurgical pain: evidence for analgesic synergy with opioids and baclofen, *Pain* 160, 1766-1780. DOI: 10.1097/j.pain.0000000000001567
- [23] Klint, J. K., Senff, S., Rupasinghe, D. B., Er, S. Y., Herzig, V., Nicholson, G. M., and King, G. F. (2012) Spider-venom peptides that target voltage-gated sodium channels: pharmacological tools and potential therapeutic leads, *Toxicon : official journal of the International Society on Toxinology* 60, 478-491. DOI: 10.1016/j.toxicon.2012.04.337
- [24] Moyer, B. D., Murray, J. K., Ligutti, J., Andrews, K., Favreau, P., Jordan, J. B., Lee, J. H., Liu, D., Long, J., Sham, K., Shi, L., Stocklin, R., Wu, B., Yin, R., Yu, V., Zou, A., Biswas, K., and Miranda, L. P. (2018) Pharmacological characterization of potent and selective Nav1.7 inhibitors engineered from Chilobrachys jingzhao tarantula venom peptide JzTx-V, *PLoS One* 13, e0196791. DOI: 10.1371/journal.pone.0196791
- [25] Flinspach, M., Xu, Q., Piekarz, A. D., Fellows, R., Hagan, R., Gibbs, A., Liu, Y., Neff, R. A., Freedman, J., Eckert, W. A., Zhou, M., Bonesteel, R., Pennington, M. W., Eddinger, K. A., Yaksh, T. L., Hunter, M., Swanson, R. V., and Wickenden, A. D. (2017) Insensitivity to pain induced by a potent selective closed-state Nav1.7 inhibitor, *Sci Rep* 7, 39662. DOI: 10.1038/srep39662
- [26] Murray, J. K., Long, J., Zou, A., Ligutti, J., Andrews, K. L., Poppe, L., Biswas, K., Moyer, B. D., McDonough, S. I., and Miranda, L. P. (2016) Single residue substitutions that confer voltage-gated sodium ion channel subtype selectivity in the Nav1.7 inhibitory peptide GpTx-1, *J Med Chem* 59, 2704-2717. DOI: 10.1021/acs.jmedchem.5b01947
- [27] Lee, C. W., Kim, S., Roh, S. H., Endoh, H., Kodera, Y., Maeda, T., Kohno, T., Wang, J. M., Swartz, K. J., and Kim, J. I. (2004) Solution structure and functional characterization of SGTx1, a modifier of Kv2.1 channel gating, *Biochemistry* 43, 890-897. DOI: 10.1021/bi0353373
- [28] Bosmans, F., Martin-Eauclaire, M. F., and Swartz, K. J. (2008) Deconstructing voltage sensor function and pharmacology in sodium channels, *Nature* 456, 202-208. DOI: 10.1038/nature07473

- [29] Osteen, J. D., Herzig, V., Gilchrist, J., Emrick, J. J., Zhang, C., Wang, X., Castro, J., Garcia-Caraballo, S., Grundy, L., Rychkov, G. Y., Weyer, A. D., Dekan, Z., Undheim, E. A., Alewood, P., Stucky, C. L., Brierley, S. M., Basbaum, A. I., Bosmans, F., King, G. F., and Julius, D. (2016) Selective spider toxins reveal a role for the Nav1.1 channel in mechanical pain, *Nature* 534, 494-499. DOI: 10.1038/nature17976
- [30] Flinspach, M. S. D., CA, US), Wickenden, Alan (San Diego, CA, US). (2016) Protoxin-II variants and methods of use, Janssen Biotech, inc. (Horsham, PA, US), United States.
- [31] Henriques, S. T., Deplazes, E., Lawrence, N., Cheneval, O., Chaousis, S., Inserra, M., Thongyoo, P., King, G. F., Mark, A. E., Vetter, I., Craik, D. J., and Schroeder, C. I. (2016) Interaction of tarantula venom peptide ProTx-II with lipid membranes is a prerequisite for its inhibition of human voltage-gated sodium channel Nav1.7, *J Biol Chem* 291, 17049-17065. DOI: 10.1074/jbc.M116.729095
- [32] Xiao, Y., Blumenthal, K., Jackson, J. O., 2nd, Liang, S., and Cummins, T. R. (2010) The tarantula toxins ProTx-II and huwentoxin-IV differentially interact with human Nav1.7 voltage sensors to inhibit channel activation and inactivation, *Mol Pharmacol* 78, 1124-1134. DOI: 10.1124/mol.110.066332
- [33] Agwa, A. J., Lawrence, N., Deplazes, E., Cheneval, O., Chen, R. M., Craik, D. J., Schroeder, C. I., and Henriques, S. T. (2017) Spider peptide toxin HwTx-IV engineered to bind to lipid membranes has an increased inhibitory potency at human voltage-gated sodium channel hNav1.7, *Biochimica et biophysica acta. Biomembranes* 1859, 835-844. DOI: 10.1016/j.bbamem.2017.01.020
- [34] Agwa, A. J., Peigneur, S., Chow, C. Y., Lawrence, N., Craik, D. J., Tytgat, J., King, G. F., Henriques, S. T., and Schroeder, C. I. (2018) Gating modifier toxins isolated from spider venom: Modulation of voltage-gated sodium channels and the role of lipid membranes, *J Biol Chem* 293, 9041-9052. DOI: 10.1074/jbc.RA118.002553
- [35] Wang, J. M., Roh, S. H., Kim, S., Lee, C. W., Kim, J. I., and Swartz, K. J. (2004) Molecular surface of tarantula toxins interacting with voltage sensors in K_v channels, *J Gen Physiol* 123, 455-467. DOI: 10.1085/jgp.200309005

- [36] Caldwell, J. H., Schaller, K. L., Lasher, R. S., Peles, E., and Levinson, S. R. (2000) Sodium channel Nav1.6 is localized at nodes of ranvier, dendrites, and synapses, *Proc Natl Acad Sci U S A* 97, 5616-5620. DOI: 10.1073/pnas.090034797
- [37] Duchen, L. W. (1970) Hereditary motor end-plate disease in the mouse: light and electron microscopic studies, *Journal of neurology, neurosurgery, and psychiatry* 33, 238-250. DOI: 10.1136/jnnp.33.2.238
- [38] Burgess, D. L., Kohrman, D. C., Galt, J., Plummer, N. W., Jones, J. M., Spear, B., and Meisler, M. H. (1995) Mutation of a new sodium channel gene, Scn8a, in the mouse mutant 'motor endplate disease', *Nat Genet* 10, 461-465. DOI: 10.1038/ng0895-461
- [39] Deuis, J., Wingerd, J., Winter, Z., Durek, T., Dekan, Z., Sousa, S., Zimmermann, K., Hoffmann, T., Weidner, C., Nassar, M., Alewood, P., Lewis, R., and Vetter, I. (2016) Analgesic effects of GpTx-1, PF-04856264 and CNV1014802 in a mouse model of Nav1.7-mediated pain, *Toxins* 8, 78. DOI: 10.3390/toxins8030078
- [40] Agwa, A. J., Henriques, S. T., and Schroeder, C. I. (2017) Gating modifier toxin interactions with ion channels and lipid bilayers: Is the trimolecular complex real?, *Neuropharmacology* 127, 32-45. DOI: 10.1016/j.neuropharm.2017.04.004
- [41] Diao, L., and Meibohm, B. (2013) Pharmacokinetics and pharmacokinetic-pharmacodynamic correlations of therapeutic peptides, *Clin Pharmacokinet* 52, 855-868. DOI: 10.1007/s40262-013-0079-0
- [42] Di, L. (2015) Strategic approaches to optimizing peptide ADME properties, *The AAPS journal* 17, 134-143. DOI: 10.1208/s12248-014-9687-3
- [43] Shen, H., Liu, D., Wu, K., Lei, J., and Yan, N. (2019) Structures of human Nav1.7 channel in complex with auxiliary subunits and animal toxins, *Science* 363, 1303-1308. DOI: 10.1126/science.aaw2493
- [44] Gennis, R. B. (2013) *Biomembranes: molecular structure and function*, Springer Science & Business Media.

- [45] Van Meer, G., Voelker, D. R., and Feigenson, G. W. (2008) Membrane lipids: where they are and how they behave, *Nat Rev Mol Cell Biol* 9, 112.
- [46] Kwan, A. H., Mobli, M., Gooley, P. R., King, G. F., and Mackay, J. P. (2011) Macromolecular NMR spectroscopy for the non-spectroscopist, *The FEBS journal* 278, 687-703. DOI: 10.1111/j.1742-4658.2011.08004.x
- [47] Deuis, J. R., Dekan, Z., Insera, M. C., Lee, T. H., Aguilar, M. I., Craik, D. J., Lewis, R. J., Alewood, P. F., Mobli, M., Schroeder, C. I., Henriques, S. T., and Vetter, I. (2016) Development of a muO-Conotoxin analogue with improved lipid membrane interactions and potency for the analgesic sodium channel Nav1.8, *J Biol Chem* 291, 11829-11842. DOI: 10.1074/jbc.M116.721662
- [48] Sali, A., and Blundell, T. L. (1993) Comparative protein modelling by satisfaction of spatial restraints, *J Mol Biol* 234, 779-815. DOI: 10.1006/jmbi.1993.1626
- [49] Morris, A. L., MacArthur, M. W., Hutchinson, E. G., and Thornton, J. M. (1992) Stereochemical quality of protein structure coordinates, *Proteins* 12, 345-364. DOI: 10.1002/prot.340120407
- [50] Maier, J. A., Martinez, C., Kasavajhala, K., Wickstrom, L., Hauser, K. E., and Simmerling, C. (2015) ff14SB: Improving the accuracy of protein side chain and backbone parameters from ff99SB, *J Chem Theory Comput* 11, 3696-3713. DOI: 10.1021/acs.jctc.5b00255

Mapping the molecular surface of the analgesic Nav1.7-selective peptide Pn3a reveals residues essential for membrane and channel interactions

Alexander Mueller, Zoltan Dekan, Quentin Kaas, Akello J. Agwa, Hana Starobova, Paul F. Alewood, Christina I. Schroeder, Mehdi Mobli, Jennifer R. Deuis and Irina Vetter

The molecular surface of the analgesic tarantula venom peptide Pn3a shows pharmacophore residues crucial for potent Nav1.7 inhibition (red) as well as residues important for proper folding (blue) and positions suitable for modification to achieve improved potency and analgesic activity (green). *In vitro* and *in vivo* pharmacology was used to obtain information on structure-activity relationships. A Pn3a-analogue with improved potency was discovered, which displays superior analgesic efficacy in *in vivo* pain models.

